Journal Pre-proofs

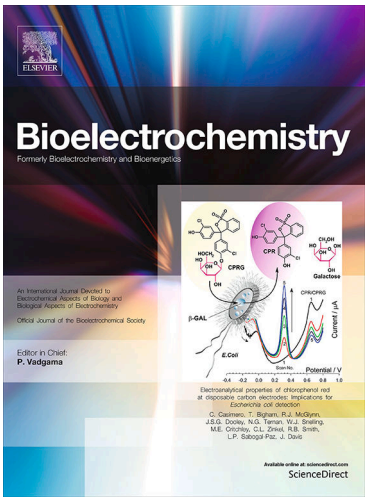

A highly sensitive flow injection amperometric glucose biosensor using a gold nanoparticles/polytyramine/Prussian blue modified screen-printed carbon electrode

Suntisak Khumngern, Ratchaneekorn Jirakunakorn, Panote Thavarungkul, Proespichaya Kanatharana, Apon Numnuam

PII: S1567-5394(20)30641-1
DOI: https://doi.org/10.1016/j.bioelechem.2020.107718
Reference: BIOJEC 107718

To appear in: *Bioelectrochemistry*

Received Date: 9 June 2020
Revised Date: 18 November 2020
Accepted Date: 21 November 2020

Please cite this article as: S. Khumngern, R. Jirakunakorn, P. Thavarungkul, P. Kanatharana, A. Numnuam, A highly sensitive flow injection amperometric glucose biosensor using a gold nanoparticles/polytyramine/Prussian blue modified screen-printed carbon electrode, *Bioelectrochemistry* (2020), doi: https://doi.org/10.1016/j.bioelechem.2020.107718

This is a PDF file of an article that has undergone enhancements after acceptance, such as the addition of a cover page and metadata, and formatting for readability, but it is not yet the definitive version of record. This version will undergo additional copyediting, typesetting and review before it is published in its final form, but we are providing this version to give early visibility of the article. Please note that, during the production process, errors may be discovered which could affect the content, and all legal disclaimers that apply to the journal pertain.

© 2020 Elsevier B.V. All rights reserved.

A highly sensitive flow injection amperometric glucose biosensor using a gold nanoparticles/polytyramine/Prussian blue modified screen-printed carbon electrode

Suntisak Khumngern[1,2,3], Ratchaneekorn Jirakunakorn[1,2,3], Panote Thavarungkul[1,2,3], Proespichaya Kanatharana[1,2,3], Apon Numnuam[1,2,3]*

[1] Center of Excellence for Trace Analysis and Biosensor, Prince of Songkla University, Hat Yai, Songkhla, 90112, Thailand

[2] Division of Physical Science, Faculty of Science, Prince of Songkla University, Hat Yai, Songkhla, 90112, Thailand

[3] Center of Excellence for Innovation in Chemistry, Faculty of Science, Prince of Songkla University, Hat Yai, Songkhla, 90112, Thailand

*Corresponding author at Division of Physical Science, Faculty of Science, Prince of Songkla University, Hat Yai, Songkhla 90112, Thailand.

Tel: +66-74-288427, Fax: +66-74-558841

*E-mail address: apon.n@psu.ac.th

Journal Pre-proofs

Highlights

- GOx chemisorbed on AuNPs/Pty/PB/SPCE displayed high affinity for glucose.
- The LOD of the biosensor was 1.0 μM, and its linear range was 1.0 μM–1.0 mM.
- The biosensor showed high operational stability over 374 injections.
- Results from this biosensor agreed well with those from the hexokinase method.

Journal Pre-proofs

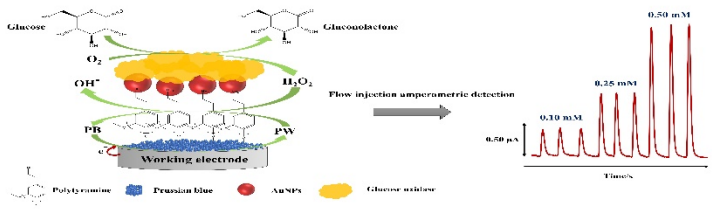

Abstract:

A novel oxidase enzyme sensor was fabricated based on the chemisorption of highly active glucose oxidase (GOx) on gold nanoparticles that were adsorbed on a polytyramine layer (AuNPs/Pty). The GOx/AuNPs/Pty assembly was coated on a Prussian blue (PB)-modified screen-printed carbon electrode (SPCE) to produce the GOx/AuNPs/Pty/PB/SPCE biosensor. The amperometric glucose biosensor response was measured at −0.10 V using a Ag pseudo-reference electrode through the reduction current of the PB mediator in a flow injection analysis system. Under optimised experimental conditions, the developed biosensor displayed linearity over the 1.0 μM–1.0 mM glucose concentration range and a limit of detection of 1.0 μM (s/n ≥ 3). A low value for the Michaelis constant of 0.21 mM indicated that the immobilised GOx had high affinity for glucose. The developed biosensor exhibited excellent operational stability over 374 injections, long-term stability over 3 weeks, good reproducibility (relative standard deviations = 1.9%–4.3%) and high selectivity. The results obtained analysing glucose in blood plasma samples were satisfactory when compared with the corresponding results recorded implementing the standard hexokinase-spectrophotometric method ($P > 0.05$).

Journal Pre-proofs

Keywords: Prussian blue; glucose; gold nanoparticles; flow injection analysis; polytyramine

Journal Pre-proofs

1. Introduction

Electrochemical enzymatic sensors, a category of electrochemical biosensors, combine the use of an enzyme, acting as a biological receptor, and an electrochemical transducer that can transform the occurrence of the reaction catalysed by the said enzyme into an appropriate signal. Amperometry is the main electrochemical technique used in these sensors, in combination with an oxidase. In these biosensors, current signals are detected and measured by application of a constant potential that drives the oxidation of hydrogen peroxide (H_2O_2) produced in the enzymatic reaction [1]. A very important factor in the development of a biosensor is the immobilisation of the receptor and various techniques have been proposed to achieve this goal [2]. Most reported approaches to enzyme immobilisation involve crosslinking, which, however, results in the loss of some enzymatic activity [3]. Therefore, the development of an enzyme immobilisation technique that does not negatively affect enzyme activity has become the focus of keen interest in the context of the research effort to fabricate new enzymatic biosensors.

Owing to its simple, reagent-less preparation approach, which results in minimal loss of enzymatic activity, immobilisation by chemisorption has attracted much attention. This method

can be employed using metal nanoparticles [3], with gold nanoparticles (AuNPs) having been commonly chosen, since thiol- and amino-containing enzymes can be immobilised on AuNPs [2, 4] with high affinity and still display high enzymatic activity [5]. AuNPs have also been proven to have excellent electrical conductivity, a large specific surface area and high biocompatibility [6, 7]. Thanks to these properties, use of AuNPs could increase enzyme loading and improve sensor response [8]. Another important technological aspect of this technique is the attachment of AuNPs to the electrode surface. This objective needs to be achieved *via* an appropriate supporting material. An attractive category of materials to be used for the said purpose are polymers, particularly those comprising free amino groups, which can coordinate AuNPs, resulting in the chemisorption of these particles. Polytyramine (Pty), a non-conducting polymer with abundant free amino groups on the Pty backbone [9, 10], is an interesting choice in the present context. Pty has been shown to easily undergo electropolymerisation onto electrode surfaces to form an extremely thin film displaying good film-forming ability and uniformity [11]; furthermore, since ultra-thin Pty films are biocompatible and environmentally friendly [12], they are a promising supporting material for AuNPs.

Besides the immobilisation strategy, an appropriate detection scheme is also important in the development of an electrochemical enzymatic sensor. Amperometric oxidase sensors most often determine H_2O_2 presence, but the sensors' signals can easily be influenced by interference from various real-sample components, since H_2O_2 detection is achieved at high oxidation potentials (about +0.60 V *vs*. Ag/AgCl) [13, 14]. In order to get around this problem, a suitable redox mediator has been employed to reduce the value of the operational potential [15, 16]. A good candidate is Prussian blue (PB) ($Fe_4^{III}[Fe^{II}(CN)_6]_3$). Due to its artificial peroxidase behaviour, it could be utilised in biosensors at low potential, while displaying good biocompatibility and

excellent catalytic activity toward H_2O_2 reduction [17]. Through this approach, the influence of interfering species was avoided [18].

We hereby report a novel oxidase sensor that combines the functions of AuNPs/Pty, acting as a support material for the immobilisation of the oxidase and PB, acting as a redox mediator. The large specific surface area of AuNPs and the enzyme chemisorption they afforded allowed high enzyme loading to be achieved, in a context whereby enzymatic activity was retained. In this study, glucose was the model analyte chosen for the development of the sensor. Notably, glucose levels in blood are related to diabetes mellitus, which is one of the most significant threats to human health, and glucose detection is very important in the early diagnosis and treatment of diabetes. In an effort to improve analyte detection performance, a flow injection analysis (FIA) system was coupled to the electrochemical sensor, an assembly known to afford analysis automation, low sample requirement and high repeatability [19–21]. Notably, the results of glucose oxidase (GOx) immobilisation by chemisorption and by crosslinking were compared. Influencing parameters were studied to achieve the highest analyte sensitivity. The analytical performance of the GOx/AuNPs/Pty/PB-modified screen-printed carbon electrode (SPCE) was then evaluated. The developed biosensor was ultimately utilised to measure glucose levels in real blood plasma samples that had not undergone pre-treatment. The results thus obtained were statistically compared with their counterparts recorded implementing the standard hospital hexokinase-spectrophotometric method.

2. Experimental

2.1. Chemicals and reagents

Journal Pre-proofs

D-(+)-glucose anhydrous, potassium chloride (KCl) and absolute ethanol were provided by Merck (Darmstadt, Germany). Glucose oxidase (GOx) from *Aspergillus niger* (EC 232-601-0, Type X-S, 155,000 units/G solid) and dopamine (DA) hydrochloride were provided by Sigma (Steinheim, Germany). Iron(III) chloride ($FeCl_3$) anhydrous was purchased from BDH (Leuven, Belgium). Hydrochloric acid (HCl) was provided by Loba Chemie (Mumbai, India). Uric acid (UA) (≥ 99%), L-ascorbic acid (AA) (99%), cholesterol (Chol) (≥ 92.5%), tyramine ($C_8H_{11}ON$), potassium hexacyanoferrate (III) ($K_3Fe(CN)_6$) and tetrachloroauric(III) acid ($HAuCl_4$) (30 wt% in dilute HCl, D = 1.637 g mL^{-1}) were provided by Sigma-Aldrich (St. Louis, USA). Potassium dihydrogen orthophosphate, di-potassium hydrogen orthophosphate and tri-sodium citrate were provided by Ajax Finechem (Sydney, Australia). All solutions were prepared using deionised (DI) water characterised by a resistance value above 15.6 MΩ cm.

2.2. Apparatus

All electrochemical experiments were conducted using an Autolab PGSTAT 128N potentiostat–galvanostat (Metrohm Autolab B.V., KM Utrecht, The Netherlands) controlled by NOVA 1.11 software. The SPCE (Metrohm, 6.1208.110) consisted of a carbon working electrode (4 mm in diameter), a carbon counter-electrode and an Ag pseudo-reference electrode. A transmission electron microscope (JEM-2010, IEOL, Japan) was employed to determine the morphology of the AuNPs. A scanning electron microscope (Quanta™ 400, FEI, USA) was employed to investigate electrode surface morphology. The electrodes' elemental composition was determined using an energy-dispersive X-ray (EDX) spectrometer (X-Max, Oxford, England). A Fourier-transform infrared (FTIR) microscope (LUMOS, Bruker, Germany) was employed to characterise the modifications that had taken place in the electrode material.

2.3. AuNPs synthesis

Journal Pre-proofs

The synthesis of AuNPs was carried out adapting the procedure employed in previous studies [22, 23]. In brief, 16.0 µL of $HAuCl_4$ were added dropwise to 50 mL of boiling ultrapure water under vigorous stirring. Au^{3+} was then reduced to Au^0 by the rapid addition of 1.0 mL of a 5.0% w/v solution of tri-sodium citrate. After the obtained mixture was boiled under stirring for 30 min, the heat was turned off and the solution allowed to cool down to room temperature. The volume of the resulting wine-red solution was adjusted to 50 mL using ultrapure water, and it was kept at 4 °C until use.

2.4. Fabrication of the glucose biosensor

The SPCE was cleaned in a saturated aqueous solution of Na_2CO_3 by applying a potential of 1.20 V to the electrode for 300 s, so as to eliminate organic binders from the surface of the SPCE [24]. The first step in the modification process (Fig. 1) was the electrodeposition of PB on the SPCE, which was realised performing 20 cycles of cyclic voltammetry (CV), scanning from −0.20 to +1.00 V at a rate of 50 mV s^{-1} in a solution containing $FeCl_3$ 2.0 mM, $K_3Fe(CN)_6$ 2.0 mM, KCl 0.10 M and HCl 20 mM. The surface of the PB-modified SPCE (PB/SPCE) was then activated by performing as many CV cycles in HCl 20 mM containing KCl 0.10 M as necessary to obtain a stable voltammogram. In order to stabilise the PB, the electrode was heated in an oven at 100 °C for 30 min [25]. Pty was then deposited on the PB/SPCE surface by electropolymerisation of tyramine implementing 10 CV cycles from −0.20 to 0.80 V at a scanning rate of 50 mV s^{-1} in phosphate buffer (pH 7.00) and ethanol (3:1) containing tyramine 20 mM. A 30-µL dispersion of AuNPs was drop-cast onto the Pty-modified PB/SPCE (Pty/PB/SPCE), which was then kept at 4 °C for 6 h to allow the AuNPs to be adsorbed onto Pty/PB/SPCE *via* the amino groups of Pty. After washing off any unbound AuNPs with DI water, 2.50 µL of the appropriate

amount of GOx (see section 3.6.2) were placed onto the modified electrode. The GOx was immobilised on the AuNPs by way of chemisorption achieved keeping the modified Pty/PB/SPCE at 4 °C overnight. Notably, the thus fabricated electrode was stored in phosphate buffer (pH 7.00) at 4 °C when not in use.

For comparison purposes, an electrode without AuNPs (GOx/Pty/PB/SPCE) was also prepared implementing the same procedure just described, using 5.0% glutaraldehyde to activate the amino group of Pty and immobilise GOx *via* crosslinking.

2.5. Electrochemical detection

CV and electrochemical impedance spectroscopy (EIS) experiments were conducted to characterise the electrodes obtained after each modification step, from bare SPCE to PB/SPCE, to Pty/PB/SPCE, to AuNPs/Pty/PB/SPCE and, finally, to GOx/AuNPs/Pty/PB/SPCE. CV experiments were performed at a scan rate of 50 mV s^{-1} in 0.10 M phosphate buffer saline (KCl 10 mM) (PBS) at pH 7.00. EIS experiments were conducted within a frequency range between 10 Hz and 0.10 kHz, with an AC amplitude of 5.0 mV and DC potential of 0.0 V in a 5.0 mM solution of $Fe(CN)_6^{3-/4-}$ containing KCl 0.10 M. The FIA system for amperometric detection used a custom-built screen-printed electrode flow cell characterised by a dead volume of 10 μL. A six-port valve (Valco Instrument, USA) was used to inject standard glucose solutions into a continuous flow of carrier buffer driven to the flow cell by a Minipuls peristaltic pump (Gilson, France) (Schematic 1).

Schematic 1 here

2.6. Optimisations

Journal Pre-proofs

The concentration of tyramine (10–40 mM) and enzyme loading (25–75 units) on the modified electrode were optimised by analysing glucose solutions characterised by a range of different concentrations (0.10, 0.25, 0.50, 0.75 and 1.00 mM) under the initial operating conditions. These conditions were such that a carrier buffer consisting of PBS 0.10 M at pH 7.00 was utilised, at a flow rate of 350 μL min^{-1}, using a sample volume of 250 μL and an operating potential of 0.00 V. Notably, the initial operating conditions were also subsequently optimised. In particular, the applied potential was made to vary between −0.20 and 0.10 V, the solution pH between 6.00 and 8.00, the sample volume between 200 and 350 μL and the flow rate between 350 and 800 μL min^{-1}. The optimal value was the one that provided a high sensitivity, as determined from the slope of the calibration curve and a short response time.

2.7. Interference

The common interfering species present in blood, that is AA, UA, DA and Chol, were studied. The relevant test was carried out by mixing glucose 5 mM with AA 0.10 mM, UA 0.50 mM, DA 12.0 nM and Chol 8.0 mM to obtain a solution that was subsequently diluted 40 times with PBS 0.10 M (pH 7.00). The signals thus obtained were compared to that obtained for glucose alone. Notably, the mentioned interfering species were at concentrations that were slightly higher than the maximum levels present in normal blood samples, whereas glucose concentration was within the normal range in blood [26].

2.8. Reproducibility and operational and long-term stability

Under the optimised analysis conditions, the reproducibility of the data furnished by six biosensors prepared on different days was studied using a series of glucose standards at 0.10, 0.25, 0.50, 0.75 and 1.00 mM concentration. Operational stability was determined by the continuous

Journal Pre-proofs

measurement of a 0.50 mM glucose solution. Finally, the electrode's long-term stability was determined by using the same enzyme electrode after storage in phosphate buffer (pH 7.00) at 4 °C for 0, 1, 2, 3, 4 and 5 weeks to analyse a series of glucose standards characterised by concentrations of 0.10, 0.25, 0.50, 0.75 and 1.00 mM.

2.9. Blood sample analyses

Blood plasma samples, as well as the relevant results of hexokinase-spectrophotometric detection, were collected from Songklanagarin Hospital, Hat Yai, Thailand. The protocol met the criteria of the Exemption Determination as was acknowledged by Human Research Ethics Committee of Faculty of Medicine, Prince of Songkla University (REC 63-480-19-2). The responses and sensitivity toward glucose standards at concentrations of 0.050, 0.10, 0.25, 0.50 and 0.75 mM in PBS 0.10 M (pH 7.00) were first compared with those of spiked plasma samples, which were prepared by pooling together 50 µL of blood plasma, 1900 µL of PBS 0.10 M at pH 7.00 and 50 µL of glucose standard solutions characterised by 2.0, 4.0, 10.0, 20.0 and 30.0 mM concentrations to produce the same final glucose concentrations as those of the glucose standards subjected to 40-fold dilution. The two sets of results obtained using the biosensor were statistically compared by Two-Way ANOVA to identify any matrix effect. The biosensor was later utilised to detect glucose in 20 plasma samples. The obtained glucose concentrations were statistically compared *via* the Wilcoxon signed-rank test to the corresponding results provided by the hospital.

3. Results and discussion

3.1. Mechanism of tyramine electropolymerisation

The cyclic voltammetric response to tyramine electropolymerisation was recorded (Supplementary information, Fig. S1). The oxidation peak current due to tyramine (□0.60 V)

Journal Pre-proofs

continuously decreased with the increasing number of scans, indicating that a non-conducting polymer was being formed on the electrode surface. The proposed mechanism of tyramine electropolymerisation is reflected by reaction (1) [10]. In particular, the electropolymerisation of tyramine monomers occurs through the compounds' *ortho* positions *via* free radical polymerisation. Firstly, the anodic oxidation of tyramine monomers produces a protonated cation radical, which is also stabilized by resonance and forms the reactive protonated radical by proton elimination. Subsequently, coupling between a protonated radical and an *ortho* carbon of the protonated cation radical leads to the formation of a dimer. This process is repeated multiple times, leading to the generation of the polymer chain.

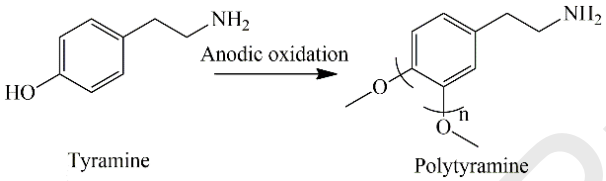

(1)

3.2. Surface morphology of the modified electrode

The scanning electron microscopy image of the surface of the bare SPCE is indicative of uniformly distributed carbon particles (Fig. 1A). Following PB deposition, sphere-like aggregations of PB particles became observable on the surface of PB/SPCE (Fig. 1B). The particulate character of the surface of the electrode was reduced when Pty was electropolymerised on top of PB/SPCE (Fig. 1C). The electrode surface became rougher following addition of AuNPs (Fig. 1D). The assembly of GOx clearly seen on the electrode surface rendered the said surface more compact and reduced its roughness (Fig. 1E). The final morphology confirmed the successful deposition of the enzyme on AuNPs/Pty/PB/SPCE. EDX mapping of AuNPs/PB/SPCE carried out before GOx immobilisation (Fig. 1F) indicated the presence of evenly distributed Au, Fe and N atoms, associated with the presence of AuNPs, PB and Pty, respectively. EDX data thus confirmed

Journal Pre-proofs

the presence of the mentioned species on the surface of SPCE. A transmission electron microscopy image and a size distribution curve (inset) indicated the average diameter of the synthesised AuNPs to be 13.9 ± 1.1 nm (n = 200) (Fig. 1G).

Fig. 1 here

3.3. Electrochemical characteristics of the different modified electrodes

The cyclic voltammetric responses of the electrode were recorded at each modification step (Fig. 2A). No redox peak was observed for the bare SPCE (curve a); by contrast, the reversible peaks typically associated with the Fe^{II}/Fe^{III} redox reaction were observed after PB deposition (curve b) [27]. Smaller redox peak currents were observed after the electropolymerisation of the non-conducting Pty (curve c); however, following the addition of AuNPs, the peak currents increased significantly in value (curve d), owing to the increase in conductivity and effective surface area of the electrode [28]. The insulating characteristics of GOx then caused the peak currents to decrease in value (curve e), indicating that the immobilisation of the enzyme on the AuNPs/PB/SPCE had been achieved.

In the Nyquist plots of different electrode modification steps, the diameter of a curve is equivalent to the value of the charge-transfer resistance (R_{ct}) and a straight line at low frequencies corresponds to the diffusion process (Fig. 2B). Related parameters calculated by fitting with the equivalent circuit model included R_{ct}, the solution resistance (R_s), the constant phase element related to double-layer charge capacitance and the Warburg impedance (Z_w) associated with the diffusion of ions between the redox probe and the electrode surface [29]. The Nyquist spectrum of each modification step was produced from three scans. The Nyquist plot of the bare SPCE was characterised by a small semicircle, corresponding to an R_{ct} value of 277.3 ± 3.0 Ω (curve a). A

significantly increased R_{ct} value was obtained after SPCE modification with PB (1485 ± 59 Ω, curve b), which hindered the charge transfer of the redox probe [30]. After Pty polymerisation, the R_{ct} value decreased to 959 ± 17 Ω (curve c), indicating that the Pty coating promoted the charge-transfer process. This observation was likely the result of the electrostatic attraction between the positively charged protonated Pty and the negatively charged redox probe [10, 31, 32]. The R_{ct} value decreased further to 406 ± 15 Ω (curve d) after AuNPs addition, due to the good conductivity of these nanoparticles. Finally, the insulating nature of the immobilised GOx caused the R_{ct} to increase again in value to 753 ± 27 Ω (curve e). Thus, the successful modification of successive layers on the SPCE was confirmed.

The electrochemical behaviour of GOx/AuNPs/Pty/PB/SPCE was characterised at scan rates ranging from 25 to 300 mV s^{-1}. The PB redox peak currents increased proportionally to the square root of the scan rate (Fig. 2C), indicating that the electrochemical kinetics of the modified electrode was controlled by diffusion of the counter K^+ into the PB lattice [33, 34, 35].

Bare SPCE, PB/SPCE, Pty/PB/SPCE and AuNPs/Pty/PB/SPCE were utilised to measure H_2O_2 concentration so as to evaluate their electrocatalytic activity toward H_2O_2 reduction (Supplementary information, Fig. S2). CV data on bare SPCE indicated a value of the H_2O_2 oxidation potential of 1.0 V (Supplementary information, Fig. S2A). When using PB/SPCE, the peak associated with PB reduction in response to H_2O_2 was observed at around −0.10 V (Supplementary information, Fig. S2B). When using Pty/PB/SPCE (Supplementary information, Fig. S2C) and AuNPs/Pty/PB/SPCE (Supplementary information, Fig. S2D) the peak associated with PB reduction was observed at −0.08 V. As a result of the excellent catalytic activity of PB, these potentials applied for the detection of H_2O_2 could eliminate the problems associated with interference from other electroactive species besides H_2O_2, for instance AA. Notably, the change

in the value of the reduction peak current was lower for Pty/PB/SPCE (Supplementary information, Fig. S2C) than for PB/SPCE (Supplementary information, Fig. S2B). This difference was due to presence of the insulating layer of Pty, which reduced the conductivity of the electrode. After electrode modification with AuNPs, the value of the change in reduction peak current increased, confirming the excellent conductivity and large specific surface area of AuNPs (Supplementary information, Fig. S2D).

The electrocatalytic behaviour of the electrode with respect to glucose was evaluated *via* CV. After the addition of glucose, the cathodic peak current associated with PB reduction increased, whereas the anodic peak current decreased (Fig. 2D). In other words, PB could be reduced to Prussian white (PW) reversibly according to reaction (2), where Fe^{II} and Fe^{III} correlate with the different oxidation states in the PB structure− PW was then oxidised by the H_2O_2 generated by the enzymatic reaction to produce PB once more (reaction (3)), which served as an electron-transfer mediator between the electrode and the H_2O_2 generated in the enzymatic reaction, leading to an increase in the cathodic current associated with PB reduction. The whole reaction course is rapid, with a constantly evolving series of reactions, a current response is produced at the electrode and quantitatively measured.

$$Fe_4^{III}[Fe^{II}(CN)_6]_3 \text{ (PB)} + 4e^- + 4K^+ \rightleftharpoons K_4Fe_4^{II}[Fe^{II}(CN)_6]_3 \text{ (PW)} \quad (2)$$

$$K_4Fe_4^{II}[Fe^{II}(CN)_6]_3 \text{ (PW)} + 2H_2O_2 \longrightarrow Fe_4^{III}[Fe^{II}(CN)_6]_3 \text{ (PB)} + 4OH^- + 4K^+ \quad (3)$$

Fig. 2 here

Journal Pre-proofs

3.4. Characterisation of AuNPs/Pty/PB/SPCE

The as-prepared Pty, PB, Pty/PB and AuNPs/Pty/PB were investigated by FTIR spectroscopy. The FTIR spectrum of Pty comprised a broad band in the 3350–3246 cm^{-1} wavenumber range that was attributed to the O–H and N–H bond stretching modes (Supplementary information, Fig. S3 (curve a)). The absorption bands at 1650–1600, 1558, 1385, 1249, 1071 and 825 and 725 cm^{-1} were attributed to the aromatic C=C bond stretching, the N–H bond bending, the angular deformation of terminal O–H and C–N bond stretching modes, the C–O–C stretching, the out-of-plane C–H deformation and inter-ring C–O–C deformation, respectively [10]. The FTIR spectrum of PB comprised a characteristic band at 2076 cm^{-1}, which corresponds to the C≡N bond stretching (Supplementary information, Fig. S3 (curve b)). Additionally, a broad band observed at 3400 cm^{-1} and an adsorption band at 1540 cm^{-1} are due to the O–H bond stretching and bending of adsorbed water, respectively [36, 37]. The FTIR spectrum of Pty/PB is characterised by similar adsorption peaks to Pty and PB (Supplementary information, Fig. S3 (curve c)). However, the peak at 1385 cm^{-1} was no longer present, whereas new absorption peaks of asymmetric aliphatic C–H stretching and N–H bond bending were observed at 2941 and 1511 cm^{-1}, respectively. These results confirmed the existence of an interaction between Pty and PB; they also indicated that the amino groups of Pty remained free on the electrode surface [38]. After adsorption of AuNPs, strong adsorption peaks at 1570 and 1392 cm^{-1} appeared, which were attributed to the symmetric and asymmetric bond stretching modes, respectively, of the carboxylate group of the citrate ion [39] (Supplementary information, Fig. S3 (curve d)). Furthermore, the absorption peak due to the C≡N bond stretching was reduced in intensity and the peak due to the N–H bond bending was no longer present. These results were evidence that a chemical bonding between AuNPs and the Pty/PB layer

had occurred. The modification of the SPCE with AuNPs/Pty/PB was thus concluded to have been successful.

3.5. Modified electrodes with and without AuNPs

The effect of immobilising GOx by chemisorption onto the AuNPs/Pty layer was compared with the effect of immobilising GOx by crosslinking directly onto the Pty layer using glutaraldehyde (in the absence of AuNPs). Electrodes with (GOx/AuNPs/Pty/PB/SPCE) and without (GOx/Pty/PB/SPCE) AuNPs were then employed to measure glucose concentration in a series of glucose standard solutions (0.10, 0.25, 0.50, 0.75 and 1.00 mM) under the initial operating conditions (see section 2.6.). The linear regression equation when GOx/Pty/PB/SPCE was used was as follows: y (μA) = (1.264 ± 0.010) x (mM) − (0.004 ± 0.005) (R^2 = 0.999); when GOx/AuNPs/Pty/PB/SPCE was used, on the other hand, it was as follows: y (μA) = (3.056 ± 0.068) x (mM) − (0.001 ± 0.031) (R^2 = 0.996). The glucose sensitivity of GOx/AuNPs/Pty/PB/SPCE was 2.4 times as high as that of GOx/Pty/PB/SPCE. Modification with AuNPs increased electrode conductivity and the increased effective surface area available for GOx immobilisation provided more active sites for the interaction with glucose. The values for the limit of detection (LOD) of the two electrodes were calculated. The LOD of GOx/Pty/PB/SPCE was 15.1 μM and that of GOx/AuNPs/Pty/PB/SPCE was 4.7 μM (s/n ≥ 3). Therefore, modification with AuNPs improved the biosensor's sensitivity and decreased the LOD value. Notably, the yield of GOx immobilisation also increased as a result of the presence of AuNPs; in particular, the results of the silver-binding assay protein method [40] indicated that the said yield improved from 52.4 ± 0.6% in the absence of AuNPs to 70.5 ± 0.1% in the presence of AuNPs. This confirmed that the chemisorption of GOx on AuNPs produced simple and reagent-less enzyme immobilization with high sensitivity.

3.6. Optimisations

3.6.1. Concentration of tyramine

The thickness of the Pty film was optimised by varying the concentration of tyramine (10, 15, 20, 25, 30 and 40 mM) in the deposition solution. The sensitivity of the calibration plot of glucose increased from 2.70 ± 0.13 μA mM^{-1}, in the case of tyramine 10 mM, to 3.280 ± 0.056 μA mM^{-1}, in the case of tyramine 20 mM (Supplementary information, Fig. S4A). The increase in sensitivity was likely caused by the increase in the number of $–NH_2$ groups available to bind AuNPs in the polymer chain. This interpretation of the evidence was indirectly confirmed by the difference in redox peak currents of the PB (ΔI) electrodeposited on the electrodes comprising and not comprising adsorbed AuNPs on the Pty layer (Supplementary information, Fig. S5 and Table S1). The observed increase in ΔI value as the concentration of tyramine increased from 10 to 20 mM indicated that the amount of adsorbed AuNPs increased with tyramine concentration. However, as tyramine concentration increased to 30 mM, the ΔI value decreased, which was likely due to the increased thickness of the Pty film, which reduced electron transfer and hindered the diffusion of substrates and products [41]. Thus, the optimal concentration of tyramine was concluded to be 20 mM.

3.6.2. Enzyme loading

Although increasing enzyme loading would increase reactivity and thus enhance response, excessive amounts of loaded enzyme are known to inhibit electron transfer due to the non-conductive nature of the enzyme [42]. With a loading of 25 units of GOx, the sensitivity was observed to be 0.553 ± 0.019 μA mM^{-1}. Sensitivity increased to 2.777 ± 0.083, 3.280 ± 0.075 and 3.31 ± 0.13 μA mM^{-1} as the enzyme loading increased to 40, 50 and 60 units, respectively

(Supplementary information, Fig. S4B). A further increment of GOx loading to 75 units reduced sensitivity. Cyclic voltammograms performed after the immobilisation of GOx onto the electrode were characterised by decreases in the redox peak currents as the GOx loading increased. This behaviour suggested that, at the GOx loading level of 75 units, the loss of electron-transfer efficiency outweighed the advantage of the increased number of active sites (Supplementary information, Fig. S6). Thus, 50 units of GOx was selected as the optimum enzyme loading.

3.6.3. Operating potential

The applied potential of amperometry is a crucial parameter affecting the system's sensitivity and selectivity. In the cyclic voltammetric response to glucose (Fig. 2D), the reduction peak of PB appeared between −0.20 and 0.10 V. With applied potentials of −0.20, −0.15 and −0.10 V, sensitivity was relatively stable at 3.63 ± 0.34 μA mM^{-1}; it then slowly started to decrease, reaching its lowest value of 1.033 ± 0.062 μA mM^{-1} at 0.10 V (Supplementary information, Fig. S4C). In order to minimise the effect of interfering signals from other electroactive compounds, which were observed as the reduction potentials increased, an applied potential of −0.10 V was selected as optimal.

3.6.4. pH of the buffer solution

Enzymatic catalysis is pH-sensitive, so amperometric responses were evaluated in the working buffer between pH 6.00 and 8.00. Electrode sensitivity at pH 6.00, 6.50 and 7.00 showed little change, with observed values of 3.582 ± 0.095, 3.503 ± 0.087 and 3.61 ± 0.13 μA mM^{-1}, respectively (Supplementary information, Fig. S4D). At pH 7.50 and 8.00, sensitivity declined slightly to 3.382 ± 0.054 and 3.347 ± 0.033 μA mM^{-1}, respectively. This decrease was likely due

to the excellent activity level of GOx between pH 4.00 and 7.00 [4]. In addition, when the pH was higher than 7.00, PB was relatively unstable, since it could be dissolved by reaction with OH^- ions [30, 43]. Hence, pH 7.00 was selected as the optimal value. Notably, this result was consistent with results reported for other glucose biosensors [44, 45].

3.6.5. Flow rate and sample volume

In FIA, the sample volume and flow rate are important parameters that affect the amount and mass transport of the substrate and the catalytic reaction time. The flow rate (350, 500, 700 and 800 μL min^{-1}) and sample volume (200, 250, 300 and 350 μL) were optimised together (Supplementary information, Fig. S7). For all sample volumes, the sensitivity of the electrode increased as the flow rate grew from 350 to 700 μL min^{-1}, as a result of the increase in mass transport of glucose from solution to the electrode surface. The reduced sample dilution also resulted in a greater response. At a flow rate of 800 μL min^{-1}, however, sensitivity decreased slightly due to the shortening of the reaction time at the mentioned high flow rate. Consequently, 700 μL min^{-1} was chosen as the optimal flow rate. As for the sample volume, electrode sensitivity at all flow rates increased from 200 to 300 μL to then level off. The reason for this observation was that reactivity increased with the sample volume; in turn, the said increase in reactivity caused the sensitivity to increase. However, once the enzyme active sites had fixed a certain amount of glucose, sensitivity could not improve. Therefore, a sample volume of 300 μL was chosen as optimal. Notably, at the optimal values for flow rate and sample volume, analysis time was 1.5 min.

3.7. Analytical performance

Journal Pre-proofs

3.7.1. Linear dynamic range and detection limit

The relationship between the reduction current and glucose concentration was linear in the 1.0 μM–1.0 mM concentration range ($R^2 = 0.999$) (Fig. 3). Sensitivity was calculated to be 16.70 ± 0.17 μA mM^{-1} cm^{-2} against the electrode surface area. The electroactive surface area of the electrode after modification with AuNPs (AuNPs/Pty/PB/SPCE) was studied *via* CV at different scan rates (Supplementary information, Fig. S8) and, using the Randles–Sevcik equation [46], was calculated to be 25.2 mm^2. The LOD and limit of quantitation (LOQ) were determined to be 1.0 μM (s/n ≥ 3) and 5.0 μM (s/n ≥ 10), respectively. In order to calculate the Michaelis constant (K_M^{app}), which indicated the reaction kinetics of the enzyme and substrate [47], the Lineweaver–Burk equation was utilised (4),

$$\frac{1}{i_c} = \frac{K_M^{app}}{i_{max}}\left(\frac{1}{C}\right) + \frac{1}{i_{max}} \quad (4)$$

where i_c is the current after the addition of glucose, i_{max} the maximum current measured in saturated glucose conditions and C is the glucose concentration. K_M^{app} was calculated by plotting $\frac{1}{i_c}$ (y axis) *versus* $\frac{1}{C}$ (x axis) in the 0.010–1.0 mM analyte concentration range. The value of the y-axis intercept (0.73 ± 0.30 μA) of the plot ($R^2 = 0.991$) represent the inverse of the i_{max} value, whereas the slope (0.1553 ± 0.0055 mM μA) is expressed by $\frac{K_M^{app}}{i_{max}}$. The K_M^{app} of the reaction between GOx and glucose was thus determined to be 0.21 mM.

In Table 1 are listed data that allow comparisons to be made between the analytical performances in glucose detection of mediated biosensors characterised by different modifications developed herein and reported in the literature. The hereby-developed biosensor exhibited the widest linear range and it also displayed a higher sensitivity than some previously described

glucose biosensors, such as the poly(*m*-phenylenediamine)-PB hybrid film [48] and the polyaniline-poly(ethylene oxide) nanocomposite modified Pt electrodes [49]. Even though the value for the sensitivity of the sensor developed in the present study was lower than the corresponding parameter of some of the previously developed sensors, such as the porous carbon and PB composite modified Pt electrode [50] and 3D silver nanocubes@PB core-shell material [51], the hereby-developed biosensor afforded a lower value for the LOD. In fact, the values for both the LOD and K_M^{app} were among the lowest in the case of the biosensor developed in the present study. In particular, the low K_M^{app} value implies that the hereby-developed biosensor had a high affinity for glucose, which means that the reaction rate will approach i_{max} quickly [47, 52]; on the other hand, the low LOD value means that use of our biosensor allows the quantification of lower levels of glucose than many of the previously reported biosensors.

Fig. 3 here

Table 1 here

3.7.2. Interference study

The potential interference of AA, UA, DA and Chol present in blood samples was investigated. No significant differences in the responses ($P > 0.05$) were observed to exist between standard glucose solutions and the corresponding mixtures (Fig. 4). In addition, no signals were observed for any of the interfering species (Supplementary information, Fig. S9). The high selectivity of the hereby-developed biosensor is due to the artificial peroxidase behaviour of the modified PB nanoparticles present on the electrode. The value of the oxidation peak potential of the generated H_2O_2 was reduced by the presence of PB nanoparticles, as described in section 3.3. In this study, glucose concentration was determined at an applied

Journal Pre-proofs

potential of −0.10 V, which is not close to the oxidation potential of the potentially interfering species mentioned above. For example, the oxidation potential of AA is about 0.30 V (*vs*. Ag/AgCl) [53]. The biosensor displayed, therefore, high selectivity for glucose in blood plasma samples.

Fig. 4 here

3.7.3. Reproducibility and operational and long-term stability

The reproducibility of the data obtained using the biosensor developed in this study was determined by measuring the glucose concentration in 0.10, 0.25, 0.50, 0.75 and 1.0 mM glucose standard solutions. The average currents of the six electrodes at each concentration were 0.377 ± 0.012, 0.949 ± 0.041, 1.974 ± 0.062, 3.101 ± 0.060 and 4.20 ± 0.11 μA for the 0.10, 0.25, 0.50, 0.75 and 1.0 mM glucose standard solutions, respectively (Fig. 5A). Values for the corresponding relative standard deviations (RSDs) were 3.2, 4.3, 3.1, 2.0 and 2.5%. These values are all much lower than the relevant value reported in the guidelines of AOAC International: 7.3% for a 10 mg L^{-1} (0.10 mM = 18 mg L^{-1}) [54].

Operational stability was tested by repeatedly analysing a 0.50 mM glucose standard solution. This concentration was chosen from the high end of the linear range (1.0 μM–1.0 mM). Stability was good up to 374 injections, with an average current response equal to 99.7 ± 2.0% of the initial response. Notably, the current response decreased to 90% after 411 injections (Fig. 5B). The operational stability of the developed biosensor was excellent because the non-conductive Pty covering improved the stability of the PB mediator [55]. The used electrode was verified by cyclic

Journal Pre-proofs

voltammetric response (Supplementary information, Fig. S10), whereby a decrease in the redox peak current of PB was evident. Therefore, the decrease in magnitude of the current response signal was due to the loss of PB during extended use in the FIA [30, 43].

The long-term stability of the electrode was tested each week over a 5-week period. The obtained sensitivities were compared with the sensitivity of the first measurement. Results indicated that the sensitivity did not change significantly during the first 3 weeks and it remained higher than 80% after 5 weeks (Fig. 5C). When compared with other biosensors (Table 1), the hereby-developed glucose biosensor was characterised by higher storage stability than most. However, some of the previously developed biosensors were reported to display higher storage stability than the hereby-developed one, including the chitosan/ionic liquid/PB-modified Pt electrode [56] and a polydopamine-GOx matrix/PB-modified glassy carbon electrode [30]. This superior stability may have to do with the implementation of the entrapment immobilisation method, which could improve the stability of the enzyme and electrode materials. However, the said method generally had limitations for mass transfer [57, 58]. Therefore, although the hereby-developed biosensor was characterised by inferior stability, it displayed superior characteristics when other performance parameters were taken into consideration. Consequently, the method employed for GOx immobilisation is a significant factor that should be carefully evaluated.

Fig. 5 here

3.7.4. Analysis of real blood plasma samples

The concentration range of glucose in human blood is 4.1–33.3 mM [26, 59] while this biosensor displayed linearity in the 1.0 μM–1.0 mM concentration range. Therefore, to perform the measurement blood plasma samples should be diluted by 33.3–4,100-fold for the analyte

Journal Pre-proofs

concentration to remain within the linear range. The dilution also helps eliminate the sample matrix effect. According to a previous study, a 40-fold dilution for plasma glucose analysis showed no matrix effect [45]. Thus a 40-fold dilution was tested. At this dilution, the sensitivities of the analyses performed on the standard glucose solutions and the spiked samples exhibited no significant difference ($P > 0.05$), indicating that there was no matrix effect (Supplementary information, Fig. S11). Accordingly, 20 human blood plasma samples were diluted 40-fold prior to the measurements and the obtained signals were utilised to determine the glucose concentration based on the standard glucose calibration equation. Results obtained utilising the developed biosensor and implementing the hexokinase method were statistically compared to each other and no significant difference was observed between the two sets of data ($P > 0.05$) (Fig. 6). This evidence confirms that the high dilution allows glucose analysis to be successfully performed within the linear range and helps to avoid the matrix effect. Values for the recovery rate of the spiked blood samples were also determined and they were observed to range from 82.5 ± 3.5% to 100.3 ± 0.4% (Table 2), in line with the values for this parameter reported in the AOAC International guidelines: 80%–110% for 10 mg L^{-1} (0.050 mM = 9 mg L^{-1}) [54]. These results indicated the high accuracy of the developed biosensor.

Fig. 6 here

Table 2 here

4. Conclusion

A novel oxidase-based enzymatic sensor for the determination of glucose concentration was successfully developed using a simple reagent-less method of enzyme immobilisation on gold nanoparticles via chemisorption. Notably, the gold nanoparticles increased the surface area of the

Journal Pre-proofs

electrode and as a result, an increased enzyme loading was possible and the electrode conductivity improved. The sensitivity of this electrode was superior to that of an electrode on which glucose oxidase had been immobilised via crosslinking, in the absence of gold nanoparticles. Immobilisation of glucose oxidase on gold nanoparticles *via* chemisorption endowed the electrode with high affinity toward glucose (K_M^{app} = 0.21 mM). A polytyramine thin film served as a supporting material for the attachment of gold nanoparticles, as it allowed nanoparticle chemisorption *via* coordination by the free amino groups of polytyramine. Also, the extremely thin polytyramine film enabled good electron transfer and substrate diffusion. Notably, PB was also utilised to modify the surface of the glucose sensor; in fact, the artificial peroxidase behaviour of PB allowed the applied operational potential to be reduced to −0.10 V, which prevented the detection of electroactive interfering compounds. Under the optimal analysis conditions, the developed biosensor exhibited excellent values for various performance parameters, including low detection limit, wide linear dynamic range, good reproducibility, good selectivity, high accuracy and high operational stability. When the developed sensor was employed for the determination of glucose concentration in blood plasma samples, the obtained results were not significantly different to those recorded implementing the standard hexokinase method ($P > 0.05$). Although the 24-h timeframe required to modify the electrode surface to obtain the described sensor is a slight drawback, one fabricated electrode could be used up to 374 times, which would help reduce analysis cost. This biosensor is a reliable device and the proposed material and immobilisation method could be used in several biosensor applications.

Acknowledgements

This project was supported by the Thailand Science Research and Innovation (TSRI) (IRN62W0002), National Research Council of Thailand, the Center of Excellence for Innovation

Journal Pre-proofs

in Chemistry (PERCH-CIC), Ministry of Higher Education, Science, Research and Innovation and the Center of Excellence for Trace Analysis and Biosensor (TAB-CoE) at Prince of Songkhla University of Thailand. We gratefully acknowledge the financial support for Suntisak Khumngern from the Science Achievement Scholarship of Thailand. The authors would like to thank Enago (www.enago.com) for the English language review and thanks also to Mr Thomas Duncan Coyne, Faculty of Science, Prince of Songkla University, Hat Yai, Songkhla, Thailand for assistance with the English text.

References

[1] S. Kurbanoglu, C. Erkmen, B. Uslu, Frontiers in electrochemical enzyme based biosensors for food and drug analysis, TrAC, Trends Anal. Chem. 124 (2020) 115809. https://doi.org/10.1016/j.trac.2020.115809

[2] H.H. Nguyen, M. Kim, An overview of techniques in enzyme immobilization, Appl. sci. convergence technol. 26 (2017) 157-163. https://doi.org/10.5757/asct.2017.26.6.157

[3] H.H. Nguyen, S.H. Lee, U.J. Lee, C.D. Fermin, M. Kim, Immobilized enzymes in biosensor applications, Mater. (Basel, Switzerland) 12 (2019) 121. https://doi.org/10.3390/ma12010121

[4] A. Samphao, P. Butmee, J. Jitcharoen, L. Svorc, G. Raber, K. Kalcher, Flow-injection amperometric determination of glucose using a biosensor based on immobilization of glucose oxidase onto Au seeds decorated on core Fe_3O_4 nanoparticles, Talanta 142 (2015) 35-42. https://doi.org/10.1016/j.talanta.2015.01.046

[5] G.A. Petkova, C.K.C. Záruba, P. Zvátora, V. Král, Gold and silver nanoparticles for biomolecule immobilization and enzymatic catalysis, Nanoscale Res. Lett. 7 (2012) 287. https://doi.org/10.1186/1556-276X-7-287

[6] W. Dang, Y. Sun, H. Jiao, L. Xu, M. Lin, AuNPs-NH_2/Cu-MOF modified glassy carbon electrode as enzyme-free electrochemical sensor detecting H_2O_2, J. Electroanal. Chem. 856 (2020) 113592. https://doi.org/10.1016/j.jelechem.2019.113592

[7] L. Zhao, J. Li, X. Chen, D. Cheng, J. Zhang, H. Yang, Highly sensitive electrochemical detection of hydrogen peroxide based on polyethyleneimine-Au nanoparticles-zinc protoporphyrin, J. Electrochem. Soc. 166 (2019) B631-B636. https://doi.org/10.1149/2.0831908jes

[8] Y. Xian, Y. Hu, F. Liu, Y. Xian, H. Wang, L. Jin, Glucose biosensor based on Au nanoparticles-conductive polyaniline nanocomposite, Biosens. Bioelectron. 21 (2006) 1996-2000. https://doi.org/10.1016/j.bios.2005.09.014

[9] M. Situmorang, J.J. Gooding, D.B. Hibbert, D. Barnett, Electrodeposited polytyramine as an immobilisation matrix for enzyme biosensors, Biosens. Bioelectron. 13 (1998) 953-962. https://doi.org/10.1016/S0956-5663(98)00033-5

[10] O. Abrahão, A.E. da Hora Machado, F.F.S. Silva, J.M. Madurro, C.M. de Castro, M.T. Sonoda, Tyramine electropolymerization revisited by DFT and experimental study, J. Mol. Struct. 1037 (2013) 200-208. https://doi.org/10.1016/j.molstruc.2012.12.056

[11] M. Yuqing, C. Jianrong, W. Xiaohua, Using electropolymerized non-conducting polymers to develop enzyme amperometric biosensors, Trends Biotechnol. 22 (2004) 227-231. https://doi.org/10.1016/j.tibtech.2004.03.004

[12] A.T.E. Vilian, V. Veeramani, S.-M. Chen, R. Madhu, C.H. Kwak, Y.S. Huh, et al., Immobilization of myoglobin on Au nanoparticle-decorated carbon nanotube/polytyramine composite as a mediator-free H_2O_2 and nitrite biosensor, Sci. Rep. 5 (2015) 18390. https://doi.org/10.1038/srep18390

[13] Z.-H. Li, H. Guedri, B. Viguier, S.-G. Sun, J.-L. Marty, Optimization of hydrogen peroxide detection for a methyl mercaptan biosensor, Sens. (Basel) 13 (2013) 5028-5039. https://doi.org/10.3390/s130405028

[14] W. Chen, S. Cai, Q.-Q. Ren, W. Wen, Y.-D. Zhao, Recent advances in electrochemical sensing for hydrogen peroxide: a review, Analyst 137 (2012) 49-58. https://doi.org/10.1039/C1AN15738H

[15] R.C. Peña, M. Bertotti, C.M.A. Brett, Methylene blue/multiwall carbon nanotube modified electrode for the amperometric determination of hydrogen peroxide, Electroanalysis 23 (2011) 2290-2296. https://doi.org/10.1002/elan.201100324

[16] S. Husmann, E. Nossol, A.J.G. Zarbin, Carbon nanotube/Prussian blue paste electrodes: Characterization and study of key parameters for application as sensors for determination of low concentration of hydrogen peroxide, Sens. Actuators, B 192 (2014) 782-790. https://doi.org/10.1016/j.snb.2013.10.074

[17] J. Wu, F. Yin, Sensitive enzymatic glucose biosensor fabricated by electrospinning composite nanofibers and electrodepositing Prussian blue film, J. Electroanal. Chem. 694 (2013) 1-5. https://doi.org/10.1016/j.jelechem.2013.02.003

[18] S. Ghaderi, M.A. Mehrgardi, Prussian blue-modified nanoporous gold film electrode for amperometric determination of hydrogen peroxide, Bioelectrochemistry 98 (2014) 64-69. https://doi.org/10.1016/j.bioelechem.2014.03.007

Journal Pre-proofs

[19] B.C. Huayhuas-Chipana, M.V. Foguel, L.M. Gonçalves, M.D.P.T. Sotomayor, Modified screen-printed electrode for the FIA-amperometric determination of 2-nitro-p-phenylenediamine, Microchem. J. 131 (2017) 92-97. https://doi.org/10.1016/j.microc.2016.11.020

[20] M. Trojanowicz, K. Kołacińska, Recent advances in flow injection analysis, Analyst 141 (2016) 2085-2139. https://doi.org/10.1039/C5AN02522B

[21] M. Trojanowicz, Recent developments in electrochemical flow detections-A review: Part I. Flow analysis and capillary electrophoresis, Anal. Chim. Acta 653 (2009) 36-58. https://doi.org/10.1016/j.aca.2009.08.040

[22] K.C. Grabar, R.G. Freeman, M.B. Hommer, M.J. Natan, Preparation and characterization of Au colloid monolayers, Anal. Chem. 67 (1995) 735-743. https://doi.org/10.1021/ac00100a008

[23] J. Turkevich, P.C. Stevenson, J. Hillier, A study of the nucleation and growth processes in the synthesis of colloidal gold, Discuss. Faraday Soc. 11 (1951) 55-75. https://doi.org/10.1039/DF9511100055

[24] G. Cui, J.H. Yoo, J.S. Lee, J. Yoo, J.H. Uhm, G.S. Cha, et al., Effect of pre-treatment on the surface and electrochemical properties of screen-printed carbon paste electrodes, The Analyst 126 (2001) 1399-1403. https://doi.org/10.1039/B102934G

[25] F. Hutanu, G. Gutt, Modified Prussian blue screen printed electrodes for H_2O_2 detection, Food Env. Saf. 12 (2016) 78-83. http://www.fia.usv.ro/fiajournal/index.php/FENS/article/view/143

[26] N. Rifai, A.R. Horvath, C.T. Wittwer, Tietz textbook of clinical chemistry and molecular diagnostics, sixth ed., Elservier, St Louis, Missouri, 2018.

[27] H. Haji-Hashemi, M.M. Habibi, M.R. Safarnejad, P. Norouzi, M.R. Ganjali, Label-free electrochemical immunosensor based on electrodeposited Prussian blue and gold nanoparticles for sensitive detection of citrus bacterial canker disease, Sens. Actuators, B 275 (2018) 61-68. https://doi.org/10.1016/j.snb.2018.07.148

[28] S. Samanman, A. Numnuam, W. Limbut, P. Kanatharana, P. Thavarungkul, Highly-sensitive label-free electrochemical carcinoembryonic antigen immunosensor based on a novel Au nanoparticles-graphene-chitosan nanocomposite cryogel electrode, Anal. Chim. Acta 853 (2015) 521-532. https://doi.org/10.1016/j.aca.2014.10.006

[29] A. Lasia, Electrochemical impedance spectroscopy and its applications, Springer, New York, 2014.

[30] Y. Lin, L. Hu, L. Yin, L. Guo, Electrochemical glucose biosensor with improved performance based on the use of glucose oxidase and Prussian Blue incorporated into a thin film of self-polymerized dopamine, Sens. Actuators, B 210 (2015) 513-518. https://doi.org/10.1016/j.snb.2014.12.107

Journal Pre-proofs

[31] M.M. Waichigo, N.D. Danielson, Ethylammonium formate as an organic solvent replacement for ion-pair reversed-phase liquid chromatography, J. Chromatogr. Sci. 44 (2006) 607-614. https://doi.org/10.1093/chromsci/44.10.607

[32] A. Küçük, O. Torul, Voltammetric sensor based on poly(3-methylthiophene) synthesized in dichloromethane for tyramine determination in moldy cheese, Synth. Met. 237 (2018) 23-28. https://doi.org/10.1016/j.synthmet.2018.01.009

[33] A.J. Bard, L.R. Faulkner, Electrochemical methods: fundamentals and applications, second ed., Wiley, 2000.

[34] F. Scholz, Electroanalytical methods: guide to experiments and applications, second ed., Springer, Berlin, Heidelberg, 2010.

[35] S. Cinti, F. Arduini, D. Moscone, G. Palleschi, AJ. Killard, Development of a Hydrogen Peroxide Sensor Based on Screen-Printed Electrodes Modified with Inkjet-Printed Prussian Blue Nanoparticles, Sensors 14 (2014) 14222-14234. https://doi.org/10.3390/s140814222

[36] H. Maaoui, P. Kumar, A. Kumar, G.-H. Pan, R. Chtourou, S. Szunerits, et al., A Prussian blue/carbon dot nanocomposite as an efficient visible light active photocatalyst for C–H activation of amines, Photochem. Photobiol. Sci. 15 (2016) 1282-1288. https://doi.org/10.1039/C6PP00203J

[37] S.N. Ghosh, Infrared spectra of the Prussian blue analogs, J. Inorg. Nucl. Chem. 36 (1974) 2465-2466. https://doi.org/10.1016/0022-1902(74)80454-9

[38] L.D. Tran, B.t. Piro, M.C. Pham, T. Ledoan, C. Angiari, L.H. Dao, et al., A polytyramine film for covalent immobilization of oligonucleotides and hybridization, Synth. Met. 139 (2003) 251-262. https://doi.org/10.1016/S0379-6779(03)00131-0

[38] J.C. Mohan, G. Praveen, K.P. Chennazhi, R. Jayakumar, S.V. Nair, Functionalised gold nanoparticles for selective induction of in vitro apoptosis among human cancer cell lines, J. Exp. Nanosci. 8 (2013) 32-45. https://doi.org/10.1080/17458080.2011.557841

[40] G. Krystal, A silver-binding assay for measuring nanogram amounts of protein in solution, Anal. Biochem. 167 (1987) 86-96. https://doi.org/10.1016/0003-2697(87)90136-9

[41] Y. Miao, J. Chen, Y. Hu, Electrodeposited nonconducting polytyramine for the development of glucose biosensors, Anal. Biochem. 339 (2005) 41-45. https://doi.org/10.1016/j.ab.2005.01.001

[42] M. Guler, V. Turkoglu, A. Kivrak, A novel glucose oxidase biosensor based on poly([2,2′;5′,2″]-terthiophene-3′-carbaldehyde) modified electrode, Int. J. Biol. Macromol. 79 (2015) 262-268. https://doi.org/10.1016/j.ijbiomac.2015.04.042

[43] A.A. Karyakin, Prussian Blue and its analogues electrochemistry and analytical applications, Electroanalysis 13 (2001) 813-819. https://doi.org/10.1002/1521-4109(200106)13:10<813::AID-ELAN813>3.0.CO;2-Z

[44] M.-H. Xue, Q. Xu, M. Zhou, J.-J. Zhu, In situ immobilization of glucose oxidase in chitosan–gold nanoparticle hybrid film on Prussian Blue modified electrode for high-sensitivity glucose detection, Electrochem. Commun. 8 (2006) 1468-1474. https://doi.org/10.1016/j.elecom.2006.07.019

[45] A. Fatoni, A. Numnuam, P. Kanatharana, W. Limbut, C. Thammakhet, P. Thavarungkul, A highly stable oxygen-independent glucose biosensor based on a chitosan-albumin cryogel incorporated with carbon nanotubes and ferrocene, Sens. Actuators, B 185 (2013) 725-734. https://doi.org/10.1016/j.snb.2013.05.056

[46] N.P. Shetti, D.S. Nayak, S.J. Malode, R.M. Kulkarni, An electrochemical sensor for clozapine at ruthenium doped TiO_2 nanoparticles modified electrode, Sens. Actuators, B 247 (2017) 858-867. https://doi.org/10.1016/j.snb.2017.03.102

[47] R.A. Kamin, G.S. Wilson, Rotating ring-disk enzyme electrode for biocatalysis kinetic studies and characterization of the immobilized enzyme layer, Anal. Chem. 52 (1980) 1198-1205. https://doi.org/10.1021/ac50058a010

[48] J.-Z. Tao, G.-R. Xu, H.-L. Hao, F.-X. Yang, K.-S. Ahn, W.-Y. Lee, Poly(m-phenylenediamine)–Prussian blue hybrid film formed by one-step electrochemical deposition for glucose biosensor, J. Electroanal. Chem. 689 (2013) 96-102. https://doi.org/10.1016/j.jelechem.2012.09.043

[49] B. Hansen, M.A. Hocevar, C.A. Ferreira, A facile and simple polyaniline-poly(ethylene oxide) based glucose biosensor, Synth. Met. 222 (2016) 224-231. https://doi.org/10.1016/j.synthmet.2016.10.028

[50] B. Thakur, X. Guo, J. Chang, M. Kron, J. Chen, Porous carbon and Prussian blue composite: A highly sensitive electrochemical platform for glucose biosensing, Sens. Biosensing Res. 14 (2017) 47-53. https://doi.org/10.1016/j.sbsr.2017.05.002

[51] P. Yang, J. Pang, F. Hu, J. Peng, D. Jiang, Z. Chu, et al., An ultrasensitive biosensing flexible chip using a novel silver@Prussian blue core-shell nanocube composite, Sens. Actuators, B 276 (2018) 31-41. https://doi.org/10.1016/j.snb.2018.08.070

[52] D.L. Nelson, M.M. Cox, Lehninger's principles of biochemistry, fourth ed., W. H. Freeman, New York, 2004.

[53] Y. Zhao, J. Zhou, Z. Jia, D. Huo, Q. Liu, D. Zhong, et al., In-situ growth of gold nanoparticles on a 3D-network consisting of a MoS_2/rGO nanocomposite for simultaneous voltammetric determination of ascorbic acid, dopamine and uric acid. Microchim. Acta 186 (2019) 92. https://doi.org/10.1007/s00604-018-3222-7

[54] AOAC International, Appendix F: guidelines for standard method performance requirements, Official Methods of Analysis, 20th ed., Rockville, MD, USA, 2016. http://www.eoma.aoac.org/app_f.pdf

[55] L.V. Lukachova, E.A. Kotel'nikova, D.D. Ottavi, E.A. Shkerin, E.E. Karyakina, D. Moscone, et al., Nonconducting polymers on Prussian Blue modified electrodes: improvement of selectivity and stability of the advanced H_2O_2 transducer, IEEE Sensors Journal, 3 (2003) 326-332. https://doi.org/10.1109/JSEN.2003.814646

[56] Y. Zhang, Y. Liu, Z. Chu, L. Shi, W. Jin, Amperometric glucose biosensor based on direct assembly of Prussian blue film with ionic liquid-chitosan matrix assisted enzyme immobilization, Sens. Actuators, B 176 (2013) 978-984. https://doi.org/10.1016/j.snb.2012.09.080

[57] I. Eş, J.D.G. Vieira, A.C. Amaral, Principles, techniques, and applications of biocatalyst immobilization for industrial application, Appl. Microbiol. Biotechnol. 99 (2015) 2065-2082. https://doi.org/10.1007/s00253-015-6390-y

[58] H.K. Kim, K.O. Lee, Y.E. Lee, Nano-immobilized biocatalysts for biodiesel production from renewable and sustainable resources, Catalysts 8 (2018) 68. https://doi.org/10.3390/catal8020068

[59] A. Adeyinka, N.P. Kondamudi, Hyperosmolar Hyperglycemic Nonketotic Coma, StatPearls, StatPearls Publishing, Treasure Island (FL), 2020.

[60] S.N. Chandra, S.S.A. Mousavi, S.H. Ng, L. Ge, S.N. Tan, A paper-based amperometric glucose biosensor developed with Prussian Blue-modified screen-printed electrodes, Sens. Actuators, B 204 (2014) 414-420. https://doi.org/10.1016/j.snb.2014.07.103

[61] X. Zhong, R. Yuan, Y.-Q. Chai, Synthesis of chitosan-Prussian blue-graphene composite nanosheets for electrochemical detection of glucose based on pseudobienzyme channeling, Sens. Actuators, B 162 (2012) 334-340. https://doi.org/10.1016/j.snb.2011.12.091

[62] D. Jiang, Z. Chu, J. Peng, W. Jin, Screen-printed biosensor chips with Prussian blue nanocubes for the detection of physiological analytes, Sens. Actuators, B 228 (2016) 679-687. https://doi.org/10.1016/j.snb.2016.01.076

[63] A.K.M. Kafi, S. Alim, R. Jose, M.M. Yusoff, Fabrication of a glucose oxidase/multiporous tin-oxide nanofiber film on Prussian blue-modified gold electrode for biosensing, J. Electroanal. Chem. 852 (2019) 113550. https://doi.org/10.1016/j.jelechem.2019.113550

[64] E. Turkmen, S.Z. Bas, H. Gulce, S. Yildiz, Glucose biosensor based on immobilization of glucose oxidase in electropolymerized poly(*o*-phenylenediamine) film on platinum nanoparticles-polyvinylferrocenium modified electrode, Electrochim. Acta 123 (2014) 93-102. https://doi.org/10.1016/j.electacta.2013.12.189

[65] A. Jędrzak, T. Rębiś, Ł. Klapiszewski, J. Zdarta, G. Milczarek, T. Jesionowski, Carbon paste electrode based on functional GOx/silica-lignin system to prepare an amperometric glucose biosensor, Sens. Actuators, B 256 (2018) 176-185. https://doi.org/10.1016/j.snb.2017.10.079

[66] R.M. Cardoso, P.R.L. Silva, A.P. Lima, D.P. Rocha, T.C. Oliveira, T.M. do Prado, et al., 3D-Printed graphene/polylactic acid electrode for bioanalysis: Biosensing of glucose and simultaneous determination of uric acid and nitrite in biological fluids, Sens. Actuators, B 307 (2020) 127621. https://doi.org/10.1016/j.snb.2019.127621

Journal Pre-proofs

[67] A. Jędrzak, T. Rębiś, M. Kuznowicz, T. Jesionowski, Bio-inspired magnetite/lignin/polydopamine-glucose oxidase biosensing nanoplatform. From synthesis, via sensing assays to comparison with others glucose testing techniques, Int. J. Biol. Macromol., 127 (2019) 677-682. https://doi.org/10.1016/j.ijbiomac.2019.02.008

Journal Pre-proofs

Table 1. A comparison of the performances of the developed glucose biosensor and other reported glucose biosensors.

Structure of biosensor	Sensitivity ($\mu A\ mM^{-1}\ cm^{-2}$)	K_M^{app} (mM)	Linear range (mM)	Applied potential (V)	LOD (μM)	Stability (%response)	Reference
GOx-PDA/PB/GCE	22.5[a]	–	0.20–3.4	0.0	46.2	60 days	[30]
GOx/CS-BSA-Fc/MWCNTs/GE	7.8[a]	1.5	0.010–30	+0.175	10	90%, 400 injections 99%, 30 days	[46]
GOx/P*m*PD-PB/GCE	28.2	1.0	0.025–0.65	0.0 (vs. SCE)	1.0	90%, 10 days	[48]
GOx/PANI-PEO/Pt electrode	16.0	–	1.0–10	+0.20	820	83%, 15 days	[49]
PCPB-GOx/Pt electrode	218.8[a]	0.44	0.030–0.4	−0.05	30	85%, 15 days	[50]
GOx/screen-printed AgNCs@PB	115.73	–	0.01–1.3	−0.05	5	77.26%, 30 days	[51]
GOx/CS/IL/PB/Pt electrode	37.8	6.6	0.01–4.2	−0.05	5	90%, 40 days	[56]
Paper-based/PB-SPCE	17.0[a]	–	0.25–2.0	−0.30	10	72%, 45 days	[60]
GOx/ConA/GOx/AuNPs/CS-PB-GR/GCE	58.7	1.29	0.025–3.2	−0.20	10	87%, 30 days	[61]
GOx/PB nanocubes/SPE	83.40	–	0.01–1.3	−0.05	10	74.1%, 3 weeks	[62]
GOx/SnO_2-NF/CS/PB/GE	–	–	0.5–5.0	−0.10	50	95%, 30 days	[63]
GOx-P*o*PD/PtNPs/$PVF^+ClO_4^-$/Pt electrode	17.40	7.6	0.06–9.64	+0.60	18	95%, 15 days	[64]
GOx-SiO_2/Lig/Fc/CPE	11.0[a]	62	0.50–9.0	+0.60	145	92%, 1 week 82%, 2 weeks	[65]
GOx/3D-printed G-PLA electrode	3.63[a]	–	0.50–6.30	+0.40	15	–	[66]
Fc/GOx/PDA/Lig/Fe_3O_4/CPE	–	6.8	10–90	+0.60	–	–	[67]
GOx/AuNPs/Pty/PB/SPCE	33.4[a] 16.7	0.21	0.0010–1.0	−0.10	1.0	99.7%, 374 injections 90%, 411 injections 99%, 3 weeks 84%, 4 weeks	This work

[a] vs. geometric surface area

P*m*PD: poly(*m*-phenylenediamine), PDA: polydopamine, ConA: concanavalin A, CS: chitosan, GR: graphene, IL: ionic liquid, BSA: bovine serum albumin, Fc: ferrocene, MWCNTs: multiwalled carbon nanotubes, GE: gold electrode, AgNCs@PB: three-dimensional silver nanocubes@Prussian blue core-shell composite, PANI-PEO: polyaniline-poly(ethylene oxide) nanocomposite, SPE: screen-printed electrode, SnO_2-NF: multiporous tin-oxide nanofiber, P*o*PD: poly(*o*-phenylenediamine), PtNPs: platinum nanoparticles, $PVF^+ClO_4^-$: polyvinylferrocenium perchlorate matrix, PCPB: porous carbon and Prussian blue composite, SiO_2/Lig: functional silica/lignin hybrid material, CPE: carbon paste electrode, GCE: glassy carbon electrode, Au electrode: gold electrode, Pt electrode: platinum electrode, G-PLA: graphene/polylactic acid, Fe_3O_4: magnetite nanoparticles.

Journal Pre-proofs

Table 2. A recovery study was performed by spiking standard solutions of glucose (0.050, 0.10, 0.25, 0.50 and 0.75 mM) into blood serum samples. After a 40-fold dilution, they were tested with the developed biosensor.

Glucose added (mM)	Total glucose found ± SD (mM), n = 3	Recovery (%), n = 3
-	0.130 ± 0.002	-
0.050	0.172 ± 0.003	82.5 ± 3.5
0.10	0.216 ± 0.003	86.2 ± 2.2
0.25	0.356 ± 0.005	90.5 ± 1.7
0.50	0.597 ± 0.009	93.4 ± 1.5
0.75	0.883 ± 0.005	100.3 ± 0.4

Journal Pre-proofs

Declaration of interests

☒ The authors declare that they have no known competing financial interests or personal relationships that could have appeared to influence the work reported in this paper.

☐The authors declare the following financial interests/personal relationships which may be considered as potential competing interests:

Journal Pre-proofs